

Broad-spectrum rejection of emerging organic contaminants with different structure and properties from complex water matrices by chlorine-resistant Janus nanofiltration membrane

Zebin Hu ¹, Kaiyue Tian ¹, Longzhe Li, Han Dai, Zhangbo Peng, Zhonglong Yin *,
Weiben Yang

Jiangsu Key Laboratory of New Power Batteries, Jiangsu Collaborative Innovation Center of Biomedical Functional Materials, School of Chemistry and Materials Science, Nanjing Normal University, Nanjing 210023, China

* Corresponding author. E-mail: 07263@njnu.edu.cn

¹ Both authors contributed equally to this work.

Number of pages: 37;

Number of Texts: 6;

Number of Figures: 23;

Number of Tables: 9;

Text S1 Reagents and chemicals

$\text{Al}(\text{NO}_3)_3 \cdot 9\text{H}_2\text{O}$, $\text{Mg}(\text{NO}_3)_2 \cdot 6\text{H}_2\text{O}$, urea, terephthalic acid (BDC), 2-amino-terephthalic acid (NH_2 -BDC), NaOCl, N, N-dimethylformamide (DMF) were purchased from Aladdin Company, Shanghai, China. Bovine serum albumin (BSA) was bought from Sigma Aldrich, USA. Polyvinylidene fluoride (PVDF) was bought from Arkema Company, French. Polyethylene glycol (PEG), glycerol, glucose, sucrose, raffinose, tetracycline (TC), norfloxacin (NOR), sulfadimidine (SM2), sulfamethoxazole (SMX), erythromycin (ERY), tobramycin (TOB), enrofloxacin (ENX), trimethoprim (TMP), 3,3',5,5'-tetrabromobisphenol A (TBBPA), dibutyl phthalate (DBP), bis(2-ethylhexyl) phthalate (DEHP), bisphenol AF (BPAF), bisphenol A (BPA), perfluorobutanoate (PFBA), nonafluorobutane-1-sulfonic acid (PFBS), perfluorooctanoic acid (PFOA), heptadecafluorononanoic acid (PFNA), triphenyl phosphate (TPHP), 2-ethylhexyl diphenyl phosphate (EHDPP), tris(2-butoxyethyl) phosphate (TBOEP), tris(2-ethylhexyl) phosphate (TEHP) and tris(2-phenylphenyl) phosphate (TBPHP) were purchased from Sinopharm Chemical Reagent Co., Ltd, China. All reagents were analytically pure and had not been further purified unless otherwise stated.

Text S2 Synthesis of 2D-MOFs and membranes

Synthesis of 2D-MOFs

Firstly, MgAl-LDH nanosheets were synthesized according to the method described by Xu et al.¹. Typically, 9.37 g of $\text{Al}(\text{NO}_3)_3 \cdot 9\text{H}_2\text{O}$ and 12.82 g of

Mg(NO₃)₂·6H₂O were dissolved in 50 mL of deionized (DI) water. Subsequently, 15.02 g of urea was added to the solution and then transferred into a stainless-steel Teflon-lined autoclave at 110 °C for 24 h. The obtained MgAl-LDH powder was washed three times with DI water and ethanol and then dried overnight at 60°C under vacuum. Then, the as-prepared MgAl-LDH (0.1 g) was dissolved in 60 mL of N, N-dimethylformamide (DMF) containing 1.2 mmol of organic ligand. The mixture was ultrasonically dissolved for 30 min. Subsequently, they were transferred into a stainless-steel Teflon-lined autoclave at certain temperature (120°C, 160°C, and 200°C) for 36 h. The obtained 2D-MOFs were washed for three times with DMF and ethanol. By modulating the organic ligand to terephthalic acid (BDC) and 2-amino-terephthalic acid (NH₂-BDC), the negatively and positively charged 2D-MOFs were obtained and denoted as MgAl-BDC-X and MgAl-BDC-NH₂-X, respectively, where X represented the synthesis temperature.

Synthesis of Janus membrane

2D-MOFs Janus NF membrane was fabricated by the nanobubble mediated nonsolvent induced phase separation (NIPS) method as described elsewhere with slight modifications ², where nanobubble was used as the porogen to generate highly porous matrix. Briefly, PVDF (3.77 g) was dissolved in 25 mL DMF and stirred thoroughly at 65°C for 12 h. Afterwards, the as-prepared charged 2D-MOFs were added to the above mixture and stirred continuously at 65°C for 6 h to obtain casting solutions A (containing MgAl-BDC-X) or B (containing MgAl-BDC-NH₂-X), then ultrasonicated for 30 min to produce nanobubbles. Subsequently, solution A was

coated onto the nonwoven fabric surface using a coating machine (HLKGM 3125, Jiangsu Shengken, China). Then it was immediately transferred into DI water bath over 24 h to obtain the negatively charged membrane. After natural drying at 25°C for 12 h, solution B was also coated on the other side of above membrane to obtain Janus membrane. The fabricated Janus membranes were denoted as JMX, where X represented the synthesis temperature of 2D-MOFs. JMX membranes with different MOFs loading (0-60 wt%) and active layer thickness of each side (100-400 μm) were also fabricated. For comparison purpose, the single-sided membranes were also constructed by coating solutions A or B into the membrane with the same total thickness of active layer with JMX, designating as SMX-N or SMX-P, where N and P represented negative and positive charge, respectively; moreover, PVDF control membrane was fabricated without adding 2D-MOFs. PVDF casting solutions in the absence of MOFs without and with nanobubble were determined by nanoparticle size and zeta potential analyzer (NS-90Z, Malvern, UK) using dynamic light scattering.

Text S3 Characterization of 2D-MOFs and membranes

Powder X-ray diffraction (PXRD) patterns were collected on an X-ray diffractometer (SmartLab, Rigaku, Japan) using Cu K α radiation ($\lambda = 1.5418 \text{ \AA}$). Nitrogen adsorption and desorption isotherm was conducted using a specific surface and pore size analyzer (ASAP 2460, Micromeritics, USA). Scanning electron microscopy (SEM, Quattro S, Thermo Fisher, USA) and transmission electron microscopy (TEM, JEM-3200, JEOL, Japan). The thickness of 2D-MOFs nanosheets

was characterized by atomic force microscopy (AFM, Brookdimenson ICON, Bruker, Germany). Fourier transform infrared spectroscopy (FTIR, 5500, Agilent, USA) and attenuated total reflection-Fourier transform infrared spectroscopy (ATR-FTIR, Nicolet IS50, Thermo Fisher, USA) were used to characterize the functional groups of materials. Water contact angle of membranes was analyzed by a contact angle analyzer (Model 190, Rame-Hart, USA). Thermo gravimetric analyzer (TGA, TG 209F1, Netzsch, Germany) was used to evaluate the thermal stability of 2D-MOFs nanosheets. Mg, Al contents were determined by inductively coupled plasma-optical emission spectrometer (ICP-OES, ICAP-6300, Thermo fisher, USA). The mechanical property of membrane was performed by Computer servo material testing machine (HZ-1004, Hengzhun, China). The molecular weight cut-off (MWCO) of the membranes was measured by filtrating of neutral molecules solutes (10 mg·L⁻¹, glycerol, glucose, sucrose, raffinose, PEG-1000, PEG-2000) with different molecular weights. Rejection ratio of neutral molecules was plotted against their MW and the MW corresponding to 90% rejection was regarded as the MWCO of membranes ³. Pore size distribution of membrane is determined by the probability density function, according to Eq. S1 and Eq. S2 ².

$$\frac{dR(r_p)}{dr_p} = \frac{1}{r_p \ln \sigma_p \sqrt{2\pi}} \exp \left[-\frac{(\ln r_p - \ln \mu_p)^2}{2(\ln \sigma_p)^2} \right] \quad (1)$$

$$r_p = 16.73 \times 10^{-3} \times M_w^{0.557} \quad (2)$$

where μ_p is the mean pore size, r_p is the Stokes radius of the neutral molecule solute, M_w is the molecular weight of each PEG solute, and σ_p is the geometric SD of the

PDF curve, which is defined as the ratio of the neutral molecular solute radius at $R = 84.13\%$ over that at $R = 50\%$.

Text S4 Water quality analysis

The concentrations of emerging contaminants (antibiotics, EDC, PFAS, OPEs) were determined using high performance liquid chromatography (HPLC, 1200 system, Agilent, USA) equipped with UV detector and chromatography column (C18 X Bridge, 250 mm×4.6 mm, 5 μ m, Waters, USA). The flow rate was 1.0 mL/min and injection volume was 20 μ L. The pH and conductivity was measured by pH meter (FE28, Mettler Toledo, Switzerland) and conductivity meter (Orion Star A212, Thermo Scientific, USA), respectively. Turbidity was measured using a turbidimeter (WGZ-200, Shanghai Xinrui, China). The dissolved organic carbon (DOC) of feed water after filtration by a 0.45 μ m membrane was determined by a total organic carbon analyzer (multi-N/C 3100, Analytik Jena, Germany). Chemical oxygen demand (COD) and biochemical oxygen demand (BOD) were measured using standard methods (State Environmental Protection Administration, 2002). Metal ion concentrations were determined by using an inductively coupled plasma optical emission spectrometer (Avio 500, PerkinElmer, USA). Each water quality parameter was the average value from triplicated parallel tests.

The bacterial rejection property of membranes was analyzed by determination of live bacteria's number in municipal wastewater after filtration using the plate count method ⁴. In brief, aliquots (0.1 mL) of diluted solutions were spread on the Luria-

Bertani (LB) agar plates and cultivated at 37°C for 2 h. The numbers of colonies on the plates were recorded for all samples. The blank control experiment was studied by cultivating the bacteria in solution without membrane filtration. The quantified bacterial rejection efficiency of membrane was calculated using Eq. S3.

$$\text{Bactericidal efficiency (\%)} = \frac{N_0 - N_1}{N_0} \times 100\% \quad (3)$$

where N_0 and N_1 were the numbers of colonies incubated by the bacteria solutions without (blank control) and with membrane filtration, respectively.

The fluorescence spectra of samples filtered through 0.22 μm polyethersulfone (PES) filters were conducted out using fluorescence spectrophotometer (F-7000, Hitachi, Japan). The ranges of excitation and emission wavelength were 200-450 and 280-550 nm, respectively. PARAFAC modeling was performed using a MATLAB toolbox, namely, DOMFluor ⁵, with a combined EEM datasets of cumulative samples of real water, real water treated with JM200 and NF270 membrane. The number of components was validated based on the split-half validation. The relative concentration of each PARAFAC component was estimated by the F_{max} output from DOMFluor. The F_{max} represents the maximum fluorescence intensity for an individual component. This fluorescence intensity was also normalized by using the Raman integration method ⁶.

Laser scanning confocal microscope measurement

After washing three times with phosphate buffered saline (PBS) solution at room temperature, membrane was stained for 30 min in the dark with nucleic acid-specific SYBR Green and α -Man and α -Glu (polysaccharide)-specific concanavalin A.

Afterwards, the stained samples was washed with PBS solution and observed using an upright microscope (Zeiss Axioplan 2, Berlin, Germany). Signals were recorded in green channels (excitation $\lambda = 488$ nm, emission $\lambda = 515/30$ nm) and red channels (excitation wavelength = 568 nm, emission wavelength = 600/50 nm). The confocal assistant software supplied by the manufacturer was used to develop 3D digitized images ⁷.

Text S5 Membrane transport principles

We used three different mass transfer models to analyze the membrane transport principles. Ferry's model describes the rejection behavior of solutes based on the relative size parameter (λ). The model is expressed as Eq. S4:

$$R = \begin{cases} [\lambda(2 - \lambda)]^2 & \lambda \leq 1 \\ 1 & \lambda > 1 \end{cases} \quad (4)$$

Where R is the rejection, and λ is the relative size parameter defined as the ratio of the solute size to the membrane pore size. When λ is less than or equal to 1, the rejection is determined by the size exclusion mechanism. As λ increases, the rejection increases due to the larger solute size relative to the pore size. When λ exceeds 1, the rejection reaches 100% as the solute size is larger than the pore size, preventing it from passing through the membrane.

The Donnan model focuses on the transport of charged solutes through a membrane. It is based on the Donnan potential ($\Delta\phi_D$) and the charge number of the solutes. The core equation is Gouy–Chapman equation as Eq. S5~9:

$$\sigma = -\epsilon\kappa\xi \frac{\sinh(\frac{F\xi}{2RT})}{\frac{F\xi}{2RT}} \quad (5)$$

$$\kappa^{-1} = \left(\frac{\epsilon RT}{2F^2 C}\right)^{1/2} \quad (6)$$

$$\frac{C_{\text{permeate}}}{C_{\text{feed}}} = \exp\left(\frac{z_A F \Delta\phi_D}{RT}\right) \quad (7)$$

$$R = \frac{C_{\text{feed}} - C_{\text{permeate}}}{C_{\text{feed}}} \quad (8)$$

$$\lambda = \frac{r_{\text{Stokes}}}{r_p} \quad (9)$$

Where κ^{-1} is Debye length, ξ (mV) is membrane zeta potential obtained through streaming potential measurements, $R=8.3145\text{J mol}^{-1} \text{K}^{-1}$ is gas constant, $F=96485 \text{ C mol}^{-1}$ is Faraday constant, $T=298\text{K}$ is absolute temperature, $\epsilon=6.933\times 10^{-10} \text{ F m}^{-1}$ is permittivity, C_{permeate} is the bulk concentration of the permeate, C_{feed} is the concentration on the inlet side (mol/m^3), R is the rejection, z_A is the contaminants charge number, $\Delta\phi_D$ is the Donnan potential, r_{stokes} is the characteristic radius of the contaminants and r_p is the characteristic radius of the membrane pore. The model indicates that the concentration ratio of the permeate to the feed is influenced by the Donnan potential, which is related to the charge properties of the solutes and the membrane. The rejection is then calculated based on the concentration difference between the feed and permeate.

The DSPM (Donnan-Steric Pore Model) model is a more comprehensive model that couples two transfer mechanisms: electromigration, and convection. The core equation of the model is Extended Nernst-Planck equation as Eq. S10~14:

$$J_i = -K_{i,d} I \left(\frac{dc_i}{dx} + \frac{z_i c_i d\psi}{RT dx} \right) + I'_{i,c} c_i J_v \quad (10)$$

$$J_i = \frac{J_v I}{A_k} \quad (11)$$

$$\begin{aligned} K_{i,d} &= 1 - 1.004\lambda_i + 0.418\lambda_i^3 + 0.21\lambda_i^4 - 0.169\lambda_i^5 \\ K_{i,c} &= \frac{3 - \phi_i^2}{2} \left(1 - \frac{\lambda_i^2}{3} \right) \end{aligned} \quad (12)$$

$$R_i = 1 - \frac{C_{i,\Delta x}^+}{C_{i,0}^-} \quad (13)$$

$$\begin{aligned} @x = 0^- \rightarrow C &= C_{i,0}^- = C_{\text{feed}} \\ @x = \Delta x^+ \rightarrow C &= C_{i,\Delta x}^+ = C_{\text{permeate}} \end{aligned} \quad (14)$$

Where J_i is the molar flux of component i , $K_{i,d}$ is the diffusion hindrance factor, D_i^∞ is the diffusion coefficient of component i in free solution, c_i is the molar concentration of component i , x is the spatial coordinate, z_i is the ionic charge number, ψ is the electrical potential, R is the ideal gas constant, T is the absolute temperature, $K_{i,c}$ is the convection transport hindrance factor, J_v is the volumetric flux (m/s), $C_{i,0}^-$ is the concentration of i at the feed-membrane interface, $C_{i,\Delta x}^+$ is the concentration of component i in the permeate solution at the downstream side of the membrane, Φ_i is volume fraction or shape factor of i , A_k is the parameter related to the membrane's sieving coefficient or reflection coefficient. The model takes into account the effects of electromigration, and convection on the transport of solutes through the membrane. The diffusion hindrance factor and convection transport hindrance factor are used to describe the influence of the membrane structure on the mass transfer mechanisms.

Ferry's model, Donnan model, and DSPM model provide different perspectives to

understand the transport behavior of solutes. Ferry's model emphasizes the size exclusion mechanism, Donnan model focuses on the charge effects, and DSPM model couples electromigration, and convection.

Text S6 The information and operating process of feed water

Due to the low concentration of EOCs in water matrices, antibiotics (TC, TOB), EDCs (TBBPA, BEZ), and PFAS (PFNA, PFOA) were spiked into feed water at 5 µg/L, respectively. Before NF treatment, the Yangtze River water underwent a flocculation process to remove suspended solid from the water. Specifically, 10 mL of AlCl_3 (20 mg·L⁻¹) was added, and the mixture was stirred at 200 rpm for 5 min, followed by stirring at 50 rpm for 15 min¹¹. The mixture was then allowed to settle for 30 min, and the insoluble matter was removed by filtration. For the Caiyue Lake water, disinfection was performed prior to NF process by adding 50 ppm of NaOCl solution (with an available chlorine concentration of 4.99%) for 1 h to prevent membrane biofouling. Municipal wastewater secondary effluent was sampled from the effluent of biological aerated filter in a municipal wastewater treatment plant in Nanjing, China. The wastewater treatment process included grid filtration, sediment by aeration tank, aerated sedimentation tank, high efficiency sedimentation tank, biological aerated filter, rotary disc filter cloth and contact disinfection (Fig. S1). Removal of bacteria, COD, BOD, metal ion and inorganic salt was also conducted and the water quality analysis methods were illustrated in Text S3. After fouling,

membrane was washed with DI water for 30 min to restore flux before next cycle. The morphology and properties of membranes after fouling and hydraulic cleaning were also determined by SEM and FTIR analyses. The leaching of 2D-MOFs into permeate was measured by inductively coupled plasma-optical emission spectrometer. Commercial NF270 membrane (Dow filmtech) was used for comparison purpose.

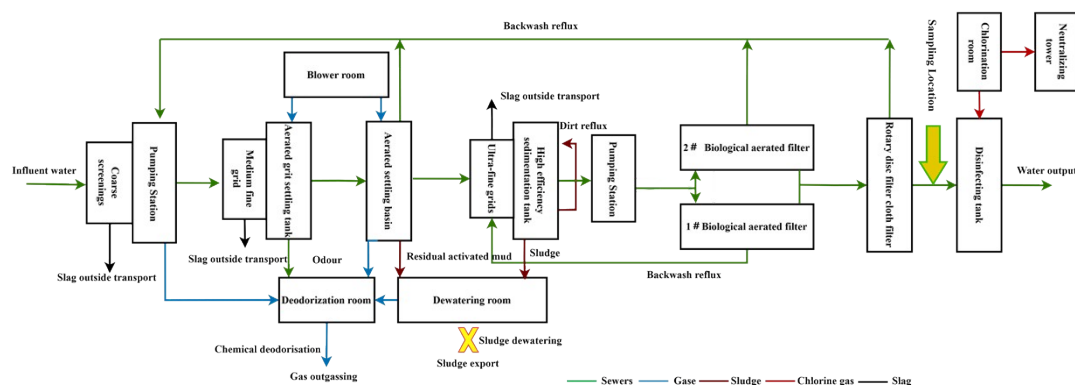


Fig. S1. The process of municipal wastewater treatment in a local wastewater treatment plant in Nanjing, China.

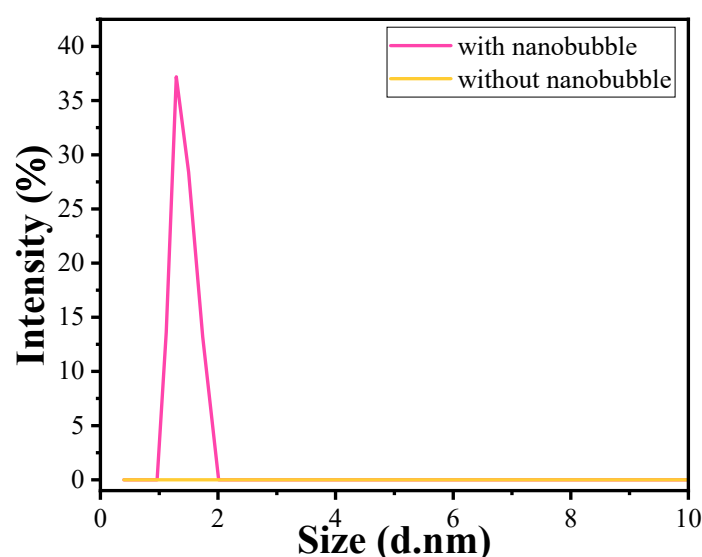


Fig. S2. Size distribution of casting solution without and with nanobubble using dynamic light scattering.

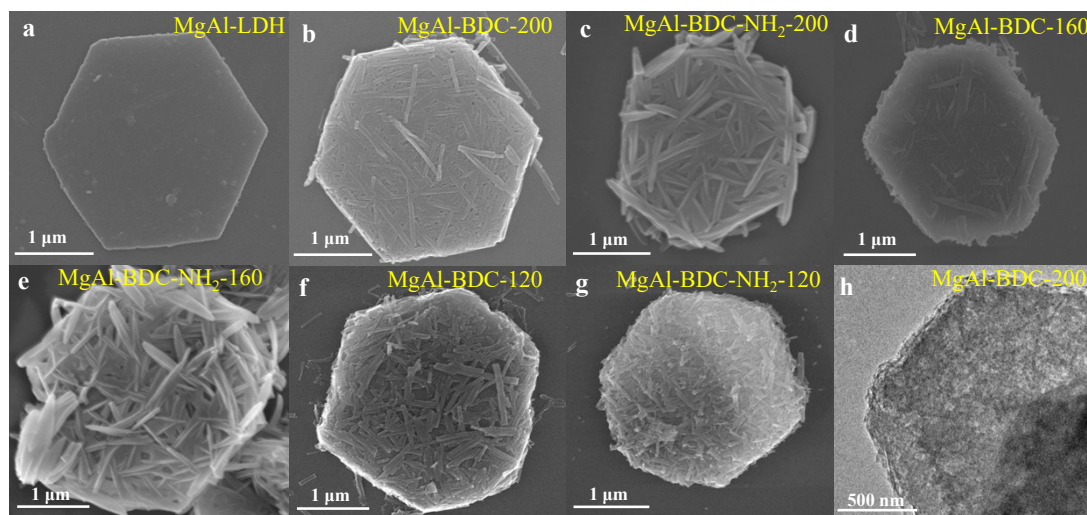


Fig. S3. SEM images of (a) MgAl-LDH, (b) MgAl-BDC-200, (c) MgAl-BDC-NH₂-200, (d) MgAl-BDC-160, (e) MgAl-BDC-NH₂-160, (f) MgAl-BDC-120, (g) MgAl-BDC-NH₂-120. TEM image of MgAl-BDC-200 (h).

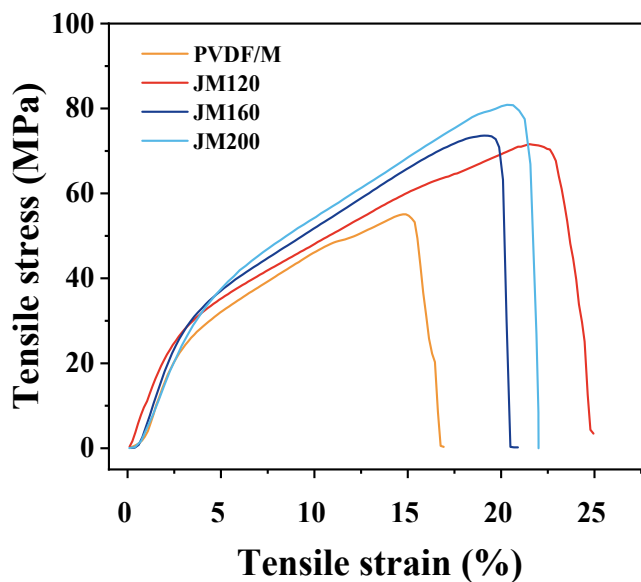


Fig. S4. Tensile strength properties of PVDF and JMX membranes.

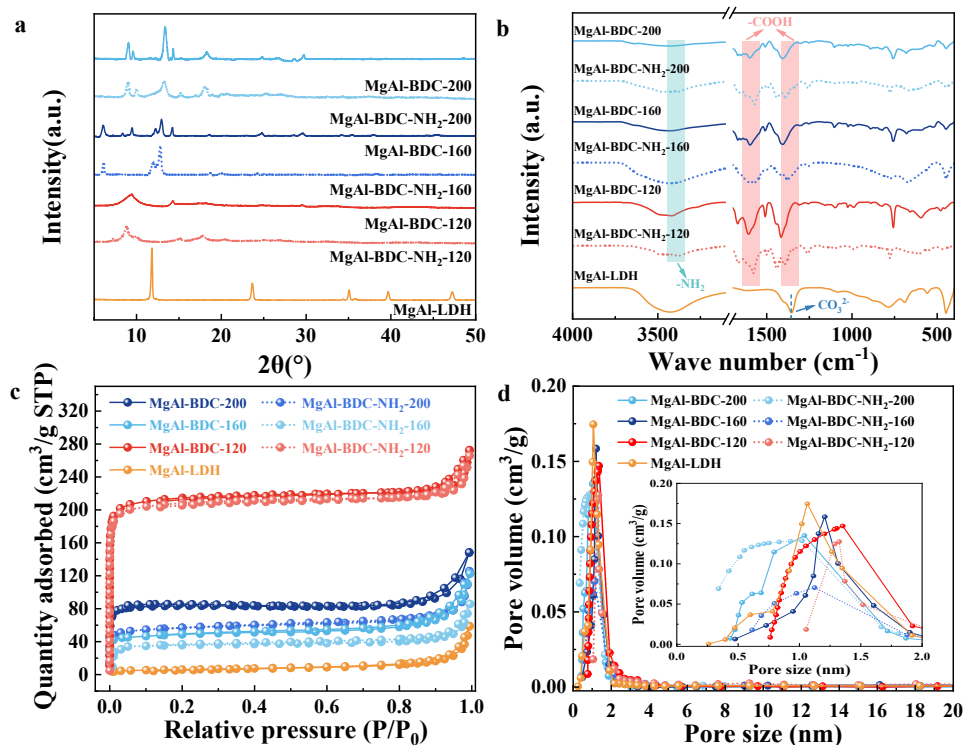


Fig. S5. Characterizations of LDH and 2D-MOFs: (a) XRD patterns, (b) FTIR spectra, (c) nitrogen adsorption-desorption isotherm curve and (d) pore size distribution.

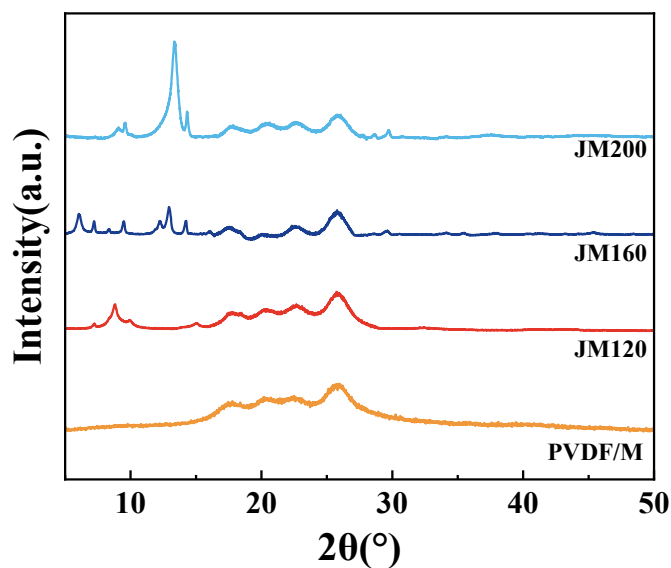


Fig. S6. XRD patterns of PVDF and JMX membranes.

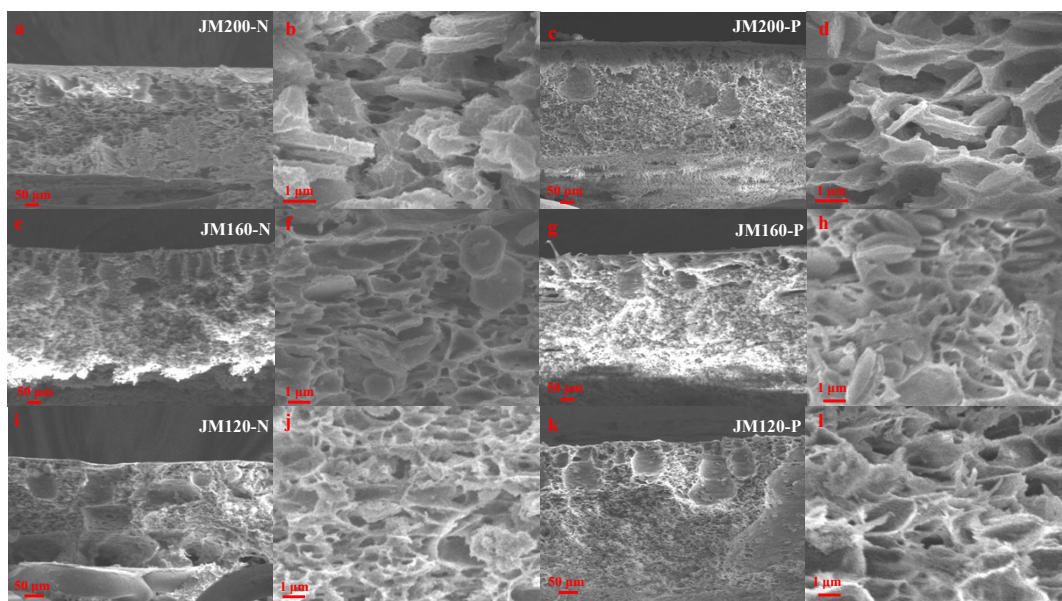


Fig. S7. Cross-sectional morphology of JMX membranes with different magnifications: (a, b) JM200-N, (c, d) JM200-P, (e, f) JM160-N, (g, h) JM160-P, (i, j) JM120-N, (k, l) JM120-P.

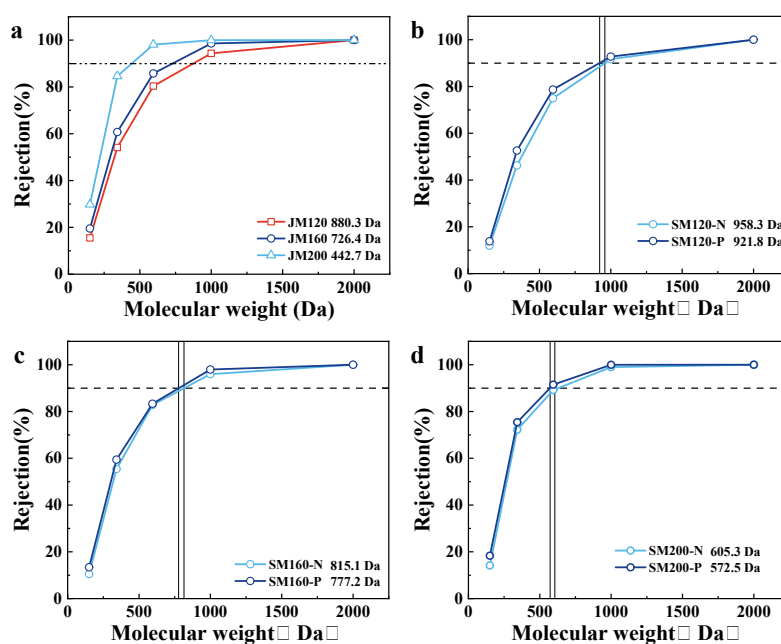


Fig. S8. MWCO of (a) Janus membranes and (b-d) corresponding single-sided membranes.

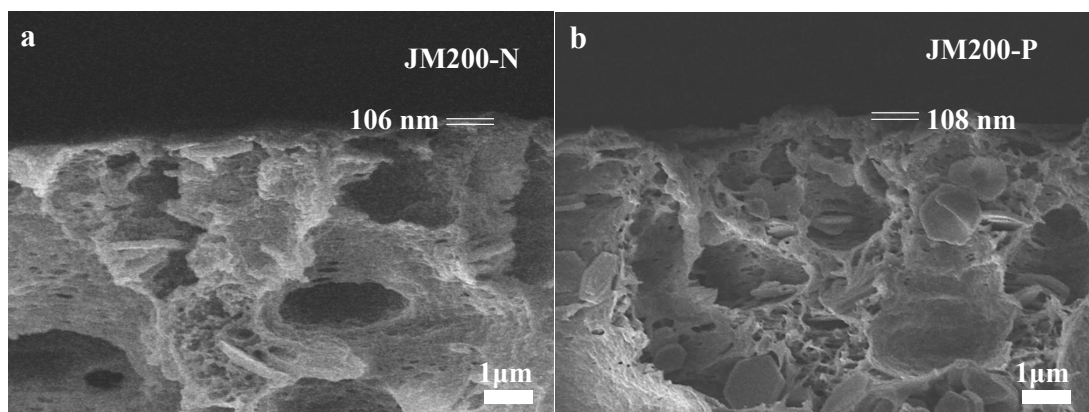


Fig. S9. The true thickness of the thin, dense skin layer at the negatively charged (a) and positively charged (b) side surface of JM200 according to the high-magnification SEM images.

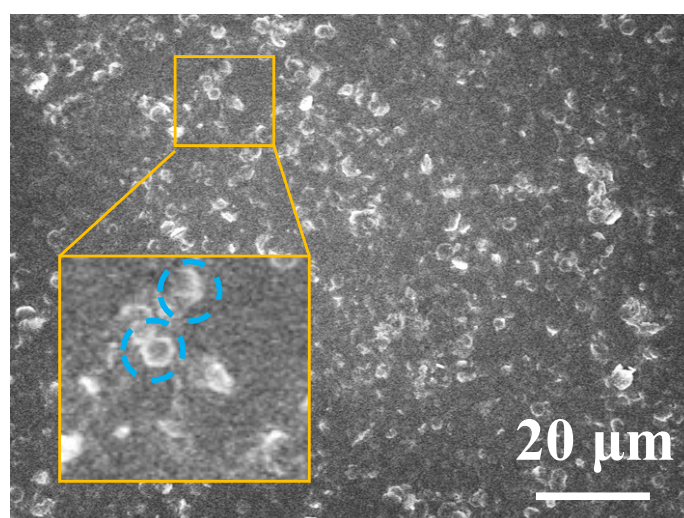


Fig. S10. Surface morphology of control JM200 made without ultrasonication.

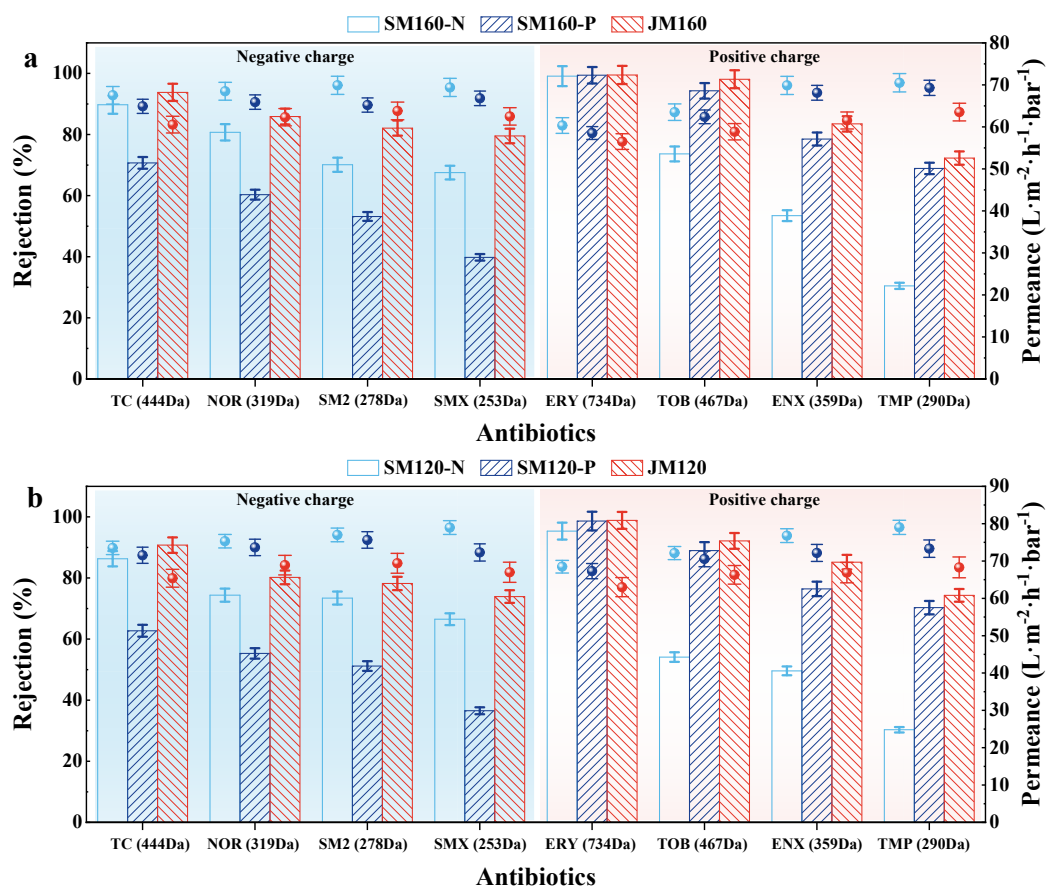


Fig. S11. Antibiotics removal performance of JM160 (a) and JM120 (b).

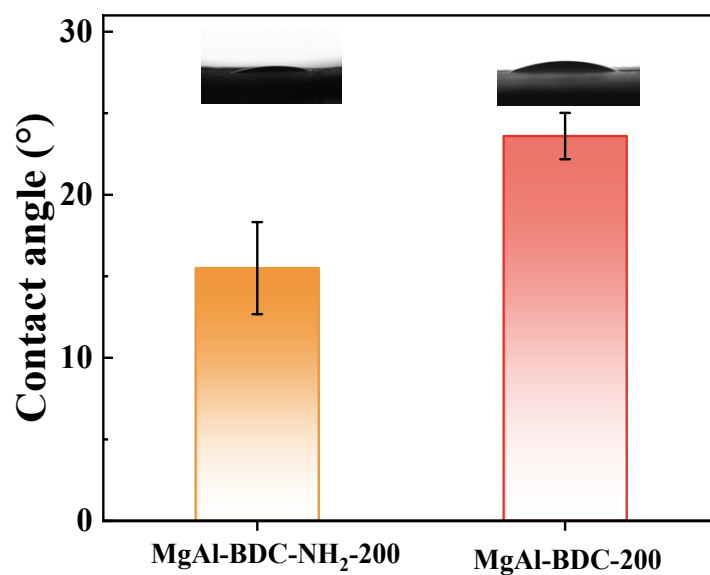


Fig. S12. Water contact angle of MgAl-BDC-NH₂-200 and MgAl-BDC-200.

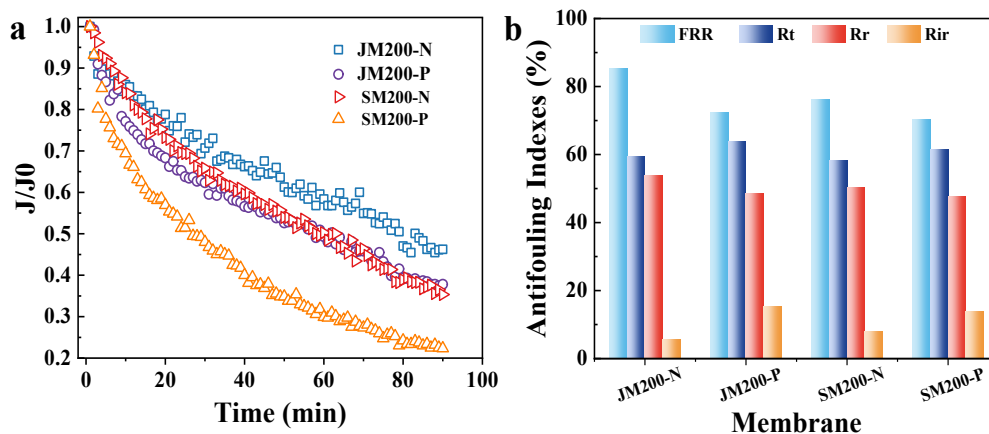


Fig. 13. Anti-fouling performance of membranes for filtration of SA (100 mg/L). Normalized flux (a) and fouling resistance (b) of Janus and single-sided membranes after fouling.

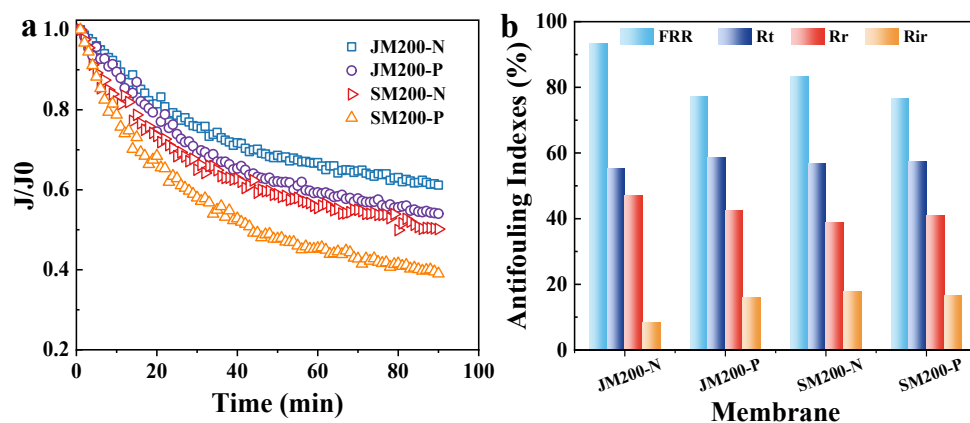


Fig. 14. Anti-fouling performance of membranes for filtration of HA (100 mg/L). Normalized flux (a) and fouling resistance (b) of Janus and single-sided membranes after fouling.

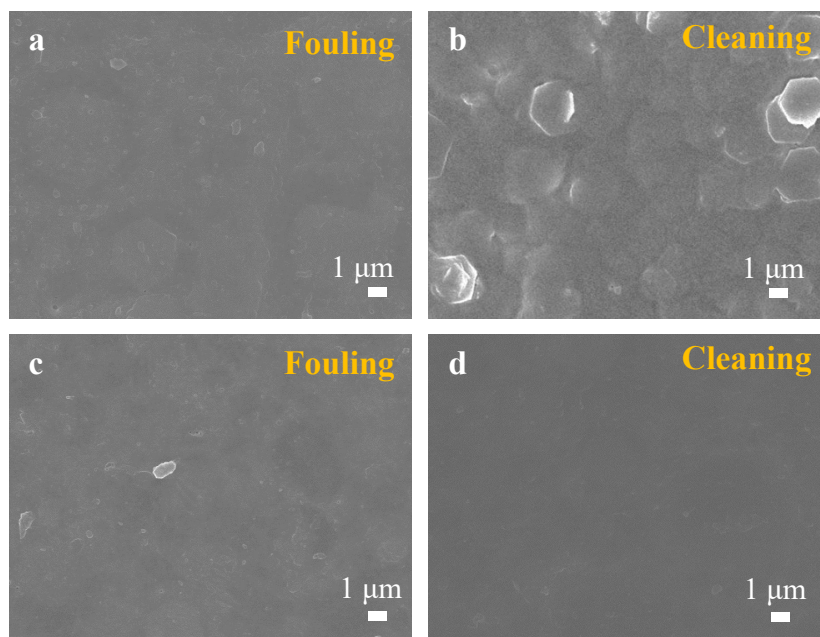


Fig. S15. SEM images of JM200-P (a, b) and JM200-N (c, d) membranes after fouling and cleaning.

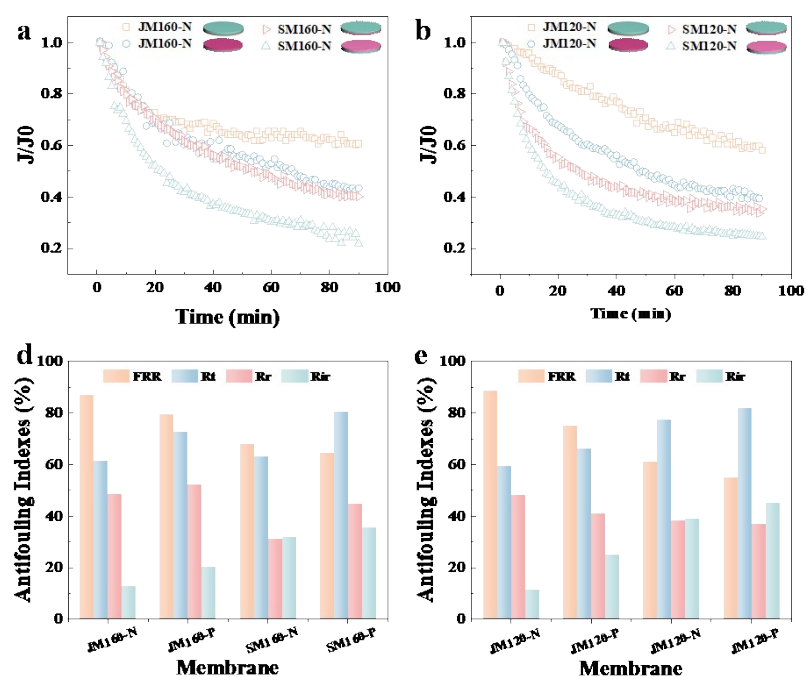


Fig. S16. Normalized flux profile (a, b) and fouling resistance (c, d) of JMX (X=120 and 160) and SMX (X=120 and 160) membranes after fouling by BSA.

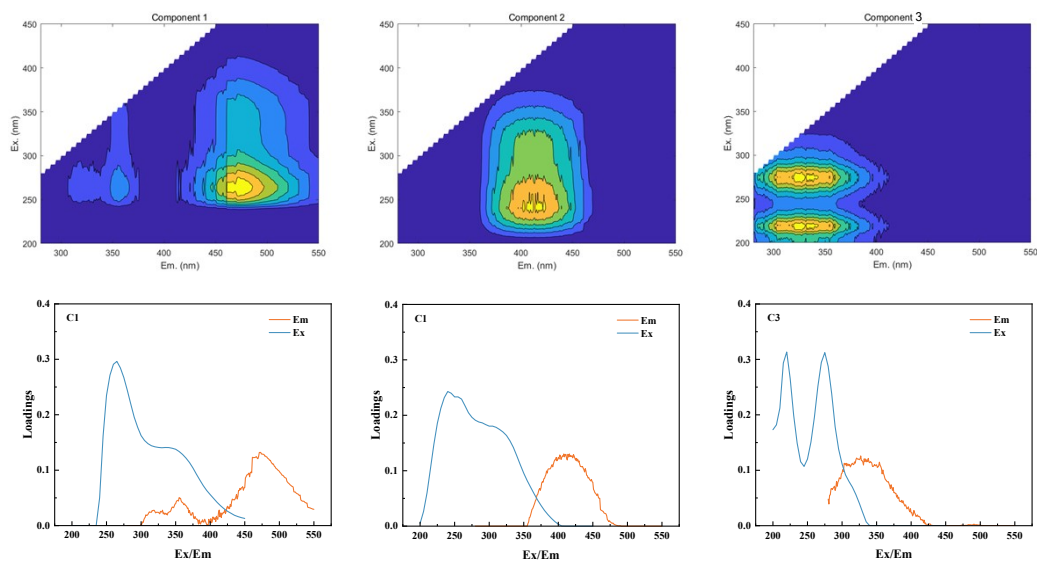


Fig. S17. PARAFAC model output showing the three fluorescent components extracted from the fluorescent EEM spectra of Caiyue Lake water and the corresponding excitation/emission loadings. C1, C2, and C3 represent the Humic-like FDOM, Tryptophan Protein-like, and Tyrosine Protein-like, respectively.

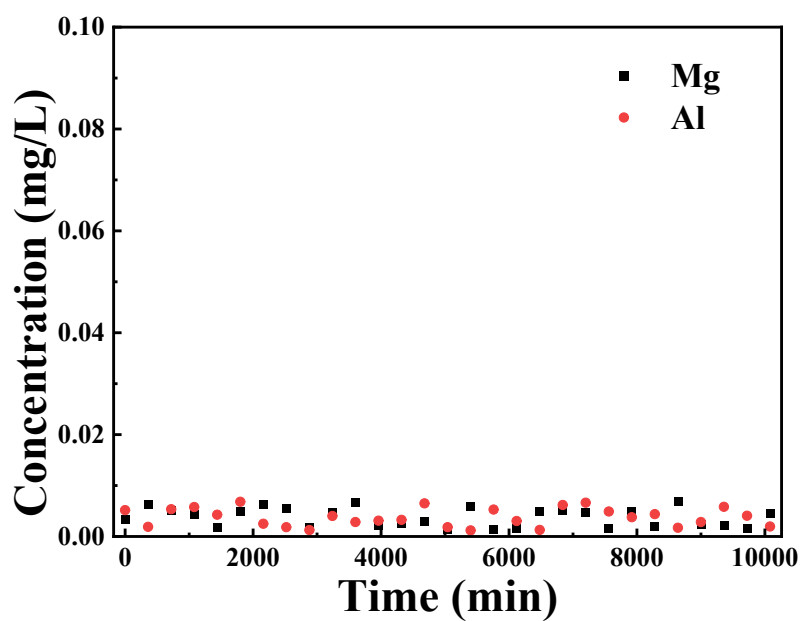


Fig. S18. The leaching of metal from JM200 during long-term filtration of Caiyue Lake water.

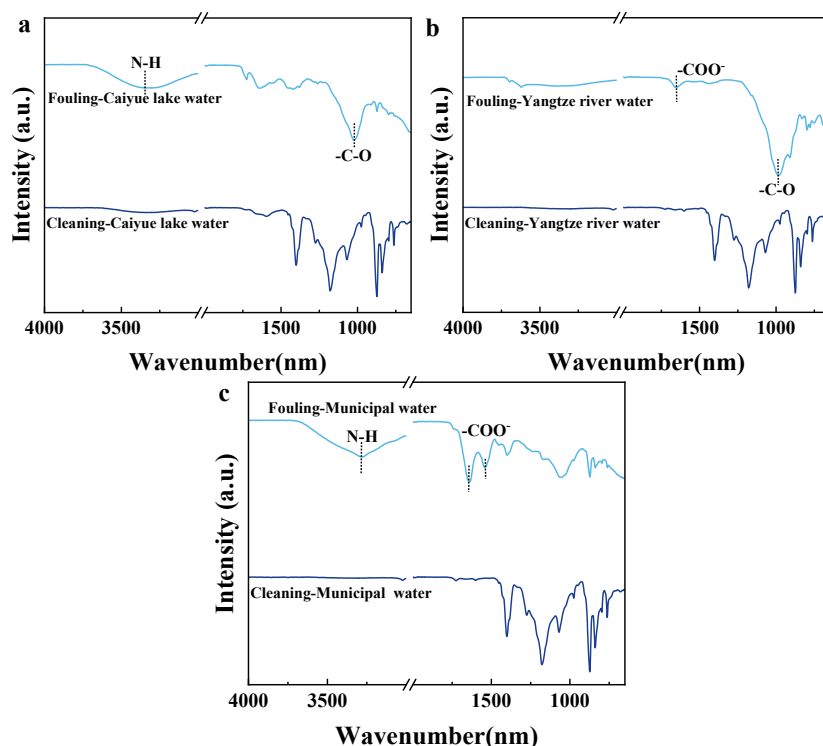


Fig. S19. JM200 membrane after fouling and hydraulic cleaning during long-term filtration of Caiyue Lake water (a), Yangtze River water (b) and municipal wastewater secondary effluent (c).

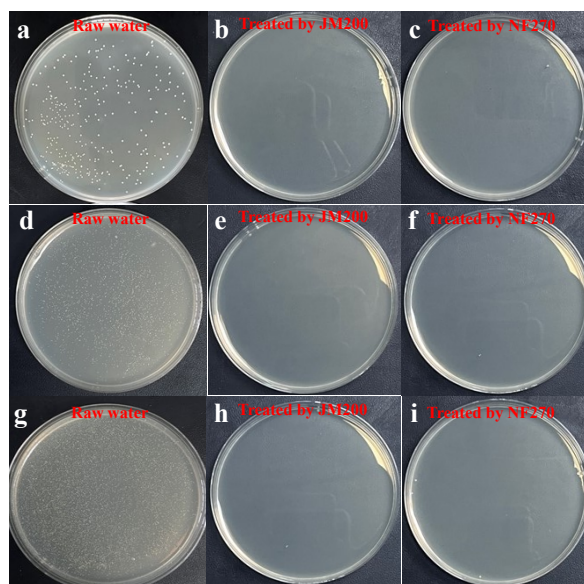


Fig. S20. Plate counting tests of raw feed water and permeate of JM200 and NF270 membranes during long-term filtration of Caiyue Lake water (a-c), Yangtze River water (d-f) and municipal wastewater secondary effluent (g-i).

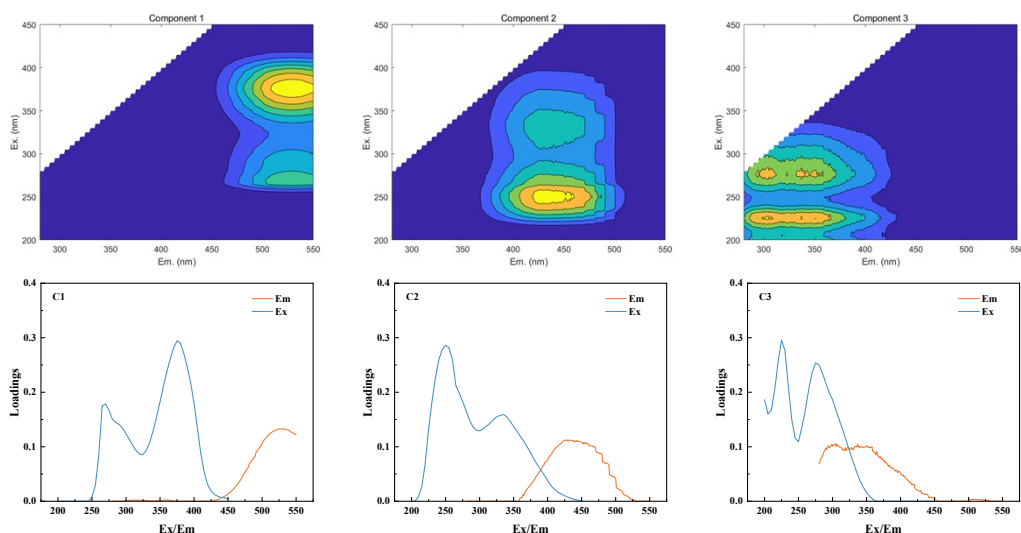


Fig. S21. PARAFAC model output showing the three fluorescent components extracted from the fluorescent EEM spectra of Yangtze River water and the corresponding excitation/emission loadings. C1, C2, and C3 represent the Humic-like FDOM, Tryptophan Protein-like, and Tyrosine Protein-like, respectively.

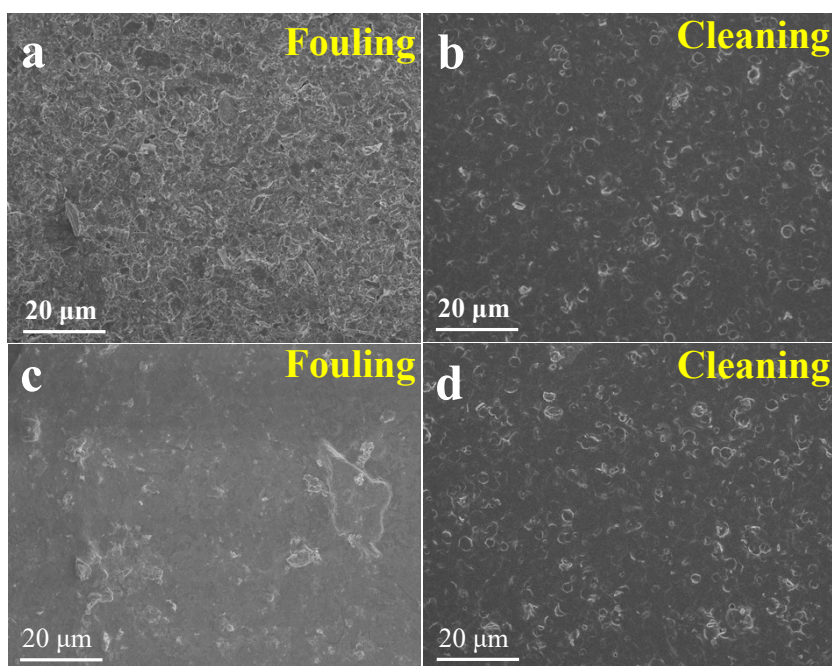


Fig. S22. SEM images of JM200 membranes after fouling and hydraulic cleaning during long-term filtration of Yangtze River water (a, b) and municipal wastewater secondary effluent (c, d).

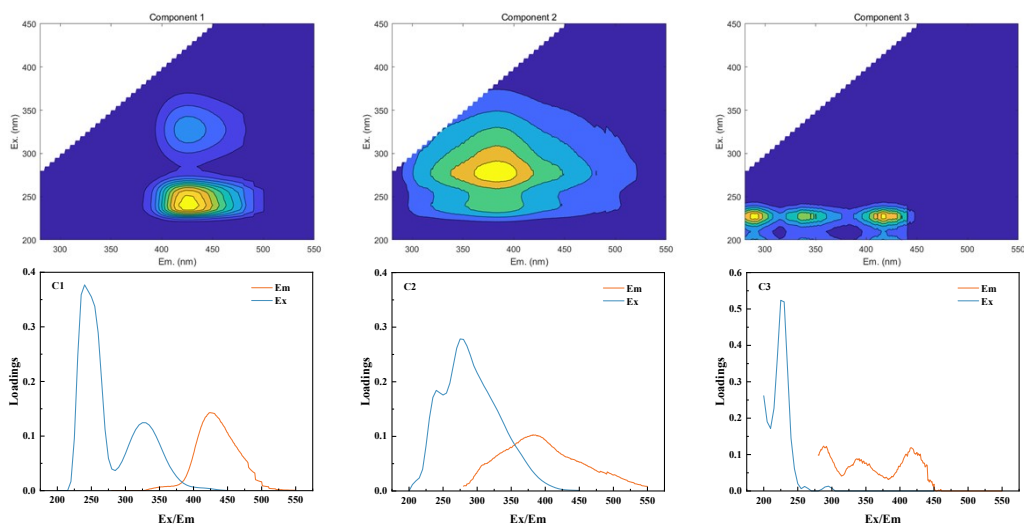
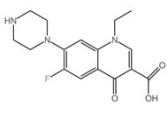
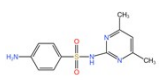
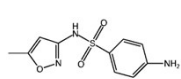
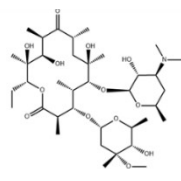
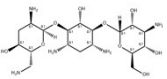
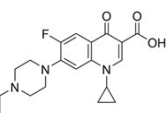
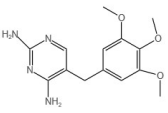
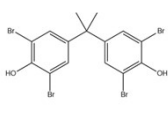
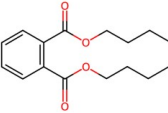
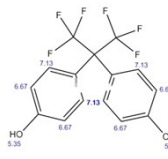


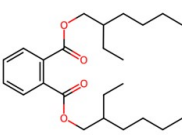
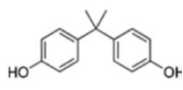
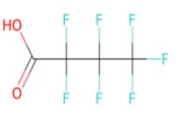
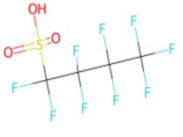
Fig. S23. PARAFAC model output showing the three fluorescent components extracted from the fluorescent EEM spectra of municipal wastewater secondary effluent and the corresponding excitation/emission loadings. C1, C2, and C3 represent the Humic-like FDOM, Tryptophan Protein-like, and Tyrosine Protein-like, respectively.


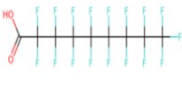
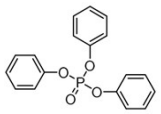
Table S1. Information of antibiotics, EDCs, PFAS and OPEs

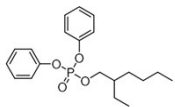
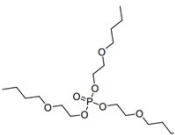
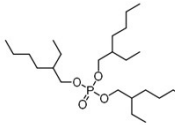
EOCs	Molecular formula	Molecular		Charge	pK _a	LogK _{ow}	R s	Structural formula
		ar	weight					
Antibiotics	Tetracycline	C ₂₂ H ₂₄ N ₂ O ₈	444.45	Negative	3.3, 7.2, 9.5	-1.33	3 8 2	

Norfl				3.1,		3	
oxaci	$C_{16}H_{18}FN_3O$	319.33	Negativ	6.1,	-0.31	.	
n	3		e	8.6		2	
						8	
				2.6		3	
Sulfa						.	
metha	$C_{12}H_{14}N_4O_2$	278.33	Negativ	5,	0.76	.	
zine	S		e	7.6		0	
				5		8	
Sulfa						2	
metho	$C_{10}H_{11}N_3O_3$		Negativ	1.6,		.	
xazol	S	253.27	e	5.7	0.48	9	
e						4	
						4	
Erythr				3.0		.	
omyci	$C_{37}H_{67}NO_{13}$	733.93	Positive	6,	2.48	8	
n				8.8		3	
						3	
				9.0,		.	
Tobra						9	
mycin	$C_{18}H_{37}N_5O_9$	467.52	Positive	10.	-5.76	2	
				4			
						3	
Enrofl	$C_{19}H_{22}FN_3O$			6.1		3	
oxaci	3	359.4	Positive	1,	0.70	.	

	n				9.0	4	
					6	6	
						3	
Trime					7.1		
thopri	C ₁₄ H ₁₈ N ₄ O ₃	290.32	Positive		0.73		
m					2	1	
						4	
	3,3,5,						
	5-					4	
Tetra							
EDCs	brom	C ₁₅ H ₁₂ Br ₄ O ₂	543.87	Negativ	7.5	7.53	
				e		2	
	obisp					0	
	henol						
	A						
Dibut						3	
yl							
Phthal	C ₁₆ H ₂₂ O ₄	278.34	Neutral		4.83		
	ate					5	
						3	
Bisph							
enol	C ₁₅ H ₁₀ F ₆ O ₂	336.23	Negativ		4.47		
			e			3	
AF						6	

PFAS	Bis(2-ethylhexylphthalate)	$C_{24}H_{38}O_4$	390.56	Neutral	-	8.71	4	
					6.7		6	
							5	
							2	
	Bisphenol A	$C_{15}H_{16}O_2$	228.3	Negative	9.6	3.3	8	
							0	
	Perfluorobutanoate (PFB A)	$C_4HF_7O_2$	214.04	Negative	0.1	2.14	7	
					7		2	
	Nonafluorobutane-1-sulfonic acid	$CF_3(CF_2)_3SO_3H$	300.1	Negative	-	1.82	3	
					3.5		1	
					7		9	

(PFB									
S)									
Perflu									
orocto									
3									
anoic									
acid	C ₇ F ₁₅ COOH	414.07	Negative	e	1.3	4.81	·	7	
(PFO									
0									
A)									
Hepta									
decafl									
uoron									
3									
onano									
ic	C ₉ HF ₁₇ O ₂	464.08	Negative	e	0.2	5.48	·	9	
Acid									
0									
(PFN									
A)									
Triph									
enyl									
3									
phosp	C ₁₈ H ₁₅ O ₄ P	326.3	/			4.7	·	3	
OPEs									
hate									
1									
/TPH									
P									

2-						
Ethyl						
hexyl						
Diphe					3	
nyl	$C_{20}H_{27}O_4P$	362.4	/	6.3	.	
Phosp					4	
hate /					8	
EHD						
PP						
Tris(2						
-						
butox					3	
yethyl	$C_{18}H_{39}O_7P$	398.5	/	3.0	.	
)					6	
phosp					3	
hate/T						
BOEP						
Tris(2					3	
-						
ethylh	$C_{24}H_{51}O_4P$	434.6	/	9.49	.	
exyl)					7	
phosp					8	

hate									
/TEH									
P									
Tris(2									
-									
pheny									
lphen									4
yl)	$C_{36}H_{27}O_4P$	554.6	/		9.99				
phosp									2
hate									4
/TBP									
HP									

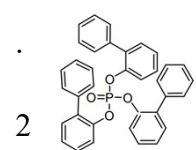


Table S2. The typical characteristics of Yangtze River water

Properties	Value	Standard
pH	7.27	6~9
Conductivity ($\mu s \cdot cm^{-1}$)	272	/
BOD ₅ (mg • L ⁻¹)	35	≤3
COD _{Cr} (mg • L ⁻¹)	16.7	≤15
DOC (mg • L ⁻¹)	13.9	/
Sulfate (mg • L ⁻¹)	33.65	≤250

Chloride (mg • L ⁻¹)	18.35	≤250
Nitrate-N (mg • L ⁻¹)	2.96	≤10
Iron (mg • L ⁻¹)	0.21	≤0.3
Manganese (mg • L ⁻¹)	0.15	≤0.1
Turbidity (NTU)	12.8	/
Total suspended solids (mg • L ⁻¹)	35.73	/
Bacteria (CFU • L ⁻¹)	10 ⁵	≤2000

Table S3. The typical characteristics of Caiyue Lake water

Properties	Value	Standard
pH	8.69	6~9
Conductivity (μs • cm ⁻¹)	260	/
BOD ₅ (mg • L ⁻¹)	32.8	≤3
COD _{Cr} (mg • L ⁻¹)	27.9	≤15
DOC (mg • L ⁻¹)	16.5	/
Sulfate (mg • L ⁻¹)	16.9	≤250
Chloride (mg • L ⁻¹)	26.85	≤250
Nitrate-N (mg • L ⁻¹)	3.84	≤10
Iron (mg • L ⁻¹)	0.22	≤0.3
Manganese (mg • L ⁻¹)	0.05	≤0.1
Turbidity (NTU)	16.9	/

Total suspended solids (mg • L ⁻¹)	23.5	/
Bacteria (CFU • mL ⁻¹)	10 ⁴	≤2000

Table S4. The typical characteristics of municipal wastewater secondary effluent

Properties	Value	Standards
pH	7.96	6~9
Conductivity ($\mu\text{s} \cdot \text{cm}^{-1}$)	549	/
BOD ₅ ($\text{mg} \cdot \text{L}^{-1}$)	35.1	≤ 3
COD _{Cr} ($\text{mg} \cdot \text{L}^{-1}$)	66.6	≤ 15
DOC ($\text{mg} \cdot \text{L}^{-1}$)	17.5	/
Sulfate ($\text{mg} \cdot \text{L}^{-1}$)	24.9	≤ 250
Chloride ($\text{mg} \cdot \text{L}^{-1}$)	43.8	≤ 250
Nitrate-N ($\text{mg} \cdot \text{L}^{-1}$)	2.81	≤ 10
Iron ($\text{mg} \cdot \text{L}^{-1}$)	0.18	≤ 0.3
Manganese ($\text{mg} \cdot \text{L}^{-1}$)	0.06	≤ 0.1
Turbidity (NTU)	6.9	/
Total suspended solids ($\text{mg} \cdot \text{L}^{-1}$)	9.87	/
Bacteria ($\text{CFU} \cdot \text{mL}^{-1}$)	10^6	≤ 2000

Table S5. Pore parameter of LDH and 2D-MOFs

Materials	Specific surface area	Average pore size (nm)
-----------	-----------------------	------------------------

	$(\text{m}^2 \cdot \text{g}^{-1})$	
MgAl-LDH	21	1.3032
MgAl-BDC-160	258	1.9282
MgAl-BDC-NH ₂ -160	188	1.8203
MgAl-BDC-200	162	1.8145
MgAl-BDC-NH ₂ -200	154	1.7604
MgAl-BDC-120	703	2.0718
MgAl-BDC-NH ₂ -120	688	1.9796

Table S6. Comparison of rejection of antibiotics and water permeance between this work and previous literature

Membrane	Permeance		$R_{\text{Antibiotic}}$ R_s (%)	R_{NaCl} (%)	Antibiotics/NaC l	Selectivity y	Ref.
	e (LMH/bar)						
PA-Mw	15.3		96.7	19.5	TC/NaCl	24.4	12
PA-H ₂ O-Mw	29.9		95.6	7.1	TC/NaCl	21.1	12
TpPa-75-250-2	50.0		97.3	16.1	TC/NaCl	31.3	13
TAPOSS-3	21		95.1	7	ERY/NaCl	19	14
PA-ZWI-6h	10		95	10	ERY/NaCl	18	15
NF90	7.2		99.0	85.5	OTC/NaCl	14.5	16
NE70	4.9		96.9	31.0	ERY/NaCl	22.3	17
PIP-TMC-SBI	10.6		95.5	6.8	ERY/NaCl	20.7	18
ZNGTFNM2	8.7		97	8	ERY/NaCl	30.7	19
PIP-TMC-	19.2		91	15	ERY/NaCl	9.44	20

AMIB						
ZNFM-0.5	10.6	91.7	7.3	ERY/NaCl	11.2	21
ZTFCMs-M3	8.4	96.5	14.4	ERY/NaCl	24.5	22
ZNFM _s	21.6	97.5	8.5	ERY/NaCl	36.6	23
PIP _{0.5γ} CD _{0.5}	26.34	97.40	17.3 3	TC/NaCl	31.8	24
JM200	47.76	98.77	5.46	TC/NaCl	76.9	This wor k

Note: TC: Tetracycline, ERY: Erythromycin, OTC: Oxytetracycline

Table S7. The water quality index of Caiyue Lake water after long-term treatment

Properties	Value (after filtration)	Standard (GB3838-2002 Grade II)
pH	7.95	6~9
Conductivity ($\mu\text{s} \cdot \text{cm}^{-1}$)	247	/
BOD ₅ ($\text{mg} \cdot \text{L}^{-1}$)	1.38	≤ 3
COD _{Cr} ($\text{mg} \cdot \text{L}^{-1}$)	3.57	≤ 15
DOC ($\text{mg} \cdot \text{L}^{-1}$)	3.58	/
Sulfate ($\text{mg} \cdot \text{L}^{-1}$)	13.7	≤ 250
Chloride ($\text{mg} \cdot \text{L}^{-1}$)	23.3	≤ 250
Nitrate-N ($\text{mg} \cdot \text{L}^{-1}$)	3.40	≤ 10

Iron ($\text{mg} \cdot \text{L}^{-1}$)	0.18	≤ 0.3
Manganese ($\text{mg} \cdot \text{L}^{-1}$)	0.04	≤ 4
Turbidity (NTU)	0.94	/
Total suspended solids ($\text{mg} \cdot \text{L}^{-1}$)	1.98	/
Bacteria ($\text{CFU} \cdot \text{mL}^{-1}$)	0	≤ 2000

Table S8. The water quality index of Yangtze River water after long-term treatment

Properties	Value (after filtration)	Standards (GB/T 18920-2020)
pH	6.94	6.97
Conductivity ($\mu\text{s} \cdot \text{cm}^{-1}$)	397	361
BOD ₅ ($\text{mg} \cdot \text{L}^{-1}$)	26.1	2.19
COD _{Cr} ($\text{mg} \cdot \text{L}^{-1}$)	48.9	2.58
DOC ($\text{mg} \cdot \text{L}^{-1}$)	13.3	5.33
Sulfate ($\text{mg} \cdot \text{L}^{-1}$)	32.94	30.7
Chloride ($\text{mg} \cdot \text{L}^{-1}$)	26.4	25.3
Nitrate-N ($\text{mg} \cdot \text{L}^{-1}$)	2.89	2.45
Iron ($\text{mg} \cdot \text{L}^{-1}$)	0.31	0.24
Manganese ($\text{mg} \cdot \text{L}^{-1}$)	0.14	0.09
Turbidity (NTU)	7.64	1.13
Total suspended solids ($\text{mg} \cdot \text{L}^{-1}$)	6.98	2.38

Bacteria (CFU • mL ⁻¹)	10 ⁴	0
------------------------------------	-----------------	---

Table S9. The water quality index of municipal wastewater secondary effluent after long-term treatment

Properties	Value (after filtration)	Standards (GB/T 18920-2020)
pH	7.76	6~9
Conductivity (μs • cm ⁻¹)	533	/
BOD ₅ (mg • L ⁻¹)	1.33	≤10
COD _{Cr} (mg • L ⁻¹)	3.9	
DOC (mg • L ⁻¹)	4.13	/
Sulfate (mg • L ⁻¹)	22.5	/
Chloride (mg • L ⁻¹)	40.7	/
Nitrate-N (mg • L ⁻¹)	2.63	/
Iron (mg • L ⁻¹)	0.14	/
Manganese (mg • L ⁻¹)	0.03	/
Turbidity (NTU)	1.05	≤10
Total suspended solids (mg • L ⁻¹)	1.56	/
Bacteria (CFU • mL ⁻¹)	0	0

Reference

- 1 X. Xu, J. Wang, A. Zhou, S. Dong, K. Shi, B. Li, J. Han and D. O'Hare, *Nat. Commun.*, 2021, **12**, 3069.
- 2 Z. Yin, Y. Liu, Z. Hu, J. Wang, F. Li and W. Yang, *J. Hazard. Mater.*, 2024, **475**, 134944.
- 3 Z. Yin, S. Zhou, M. Hu, Z. Yang and W. Yang, *J. Membr. Sci.*, 2022, **650**, 120394.
- 4 Z. Hu, Z. Yin, Y. Chen, T. Wen, F. Li and W. Yang, *J. Membr. Sci.*, 2024, **709**, 123108.
- 5 T. Maqbool, M. Sun, L. Chen and Z. Zhang, *Water Res.*, 2022, **210**, 117979.
- 6 K. D. B. Kathleen R. Murphy, Robert G. M. Spencer, Colin A. Stedmon, Jennifer R. Boehme, George R. Aiken., *Environ. Sci. Technol.*, 2010, **44**, 9405-9412.
- 7 L. Peng, H. Zhu, H. Wang, Z. Guo, Q. Wu, C. Yang and H. Y. Hu, *Nat. Commun.*, 2023, **14**, 5734.
- 8 C. Liu, L. Chen and L. Zhu, *Water Res.*, 2017, **119**, 33-46.
- 9 C.-C. Ji, K.-Y. Chen, S.-K. Deng, J.-X. Wang, Y.-X. Hu, X.-H. Xu and L.-H. Cheng, *Water Res.*, 2023, **229**, 119395.
- 10 L. Wang, S. Xu and J. Li, *Environ. Sci. Technol.*, 2011, **45**, 9566-9573.
- 11 Z. Yin, C. Yang, C. Long and A. Li, *Chem. Eng. J.*, 2018, **332**, 109-117.
- 12 B.-Q. Huang, Y.-J. Tang, Z.-X. Zeng, S.-M. Xue, S.-Q. Li, Y.-R. Wang, E.-C. Li, C. Y. Tang and Z.-L. Xu, *J. Membr. Sci.*, 2021, **629**, 119285.
- 13 Y. Pan, H. Liu, Z. Huang, W. Zhang, H. Gao, L. Liang, L. Dong and H. Meng, *Angew Chem. Int. Ed. Engl.*, 2024, **63**, e202316315.

- 14 Y.-J. Shen, Q.-R. Kong, L.-F. Fang, Z.-L. Qiu and B.-K. Zhu, *J. Membr. Sci.*, 2021, **623**, 119044.
- 15 Y.-S. Guo, Y.-L. Ji, B. Wu, N.-X. Wang, M.-J. Yin, Q.-F. An and C.-J. Gao, *J. Membr. Sci.*, 2020, **593**, 117441.
- 16 K. Košutić, D. Dolar, D. Ašperger and B. Kunst, *Sep. Purif. Technol.*, 2007, **53**, 244-249.
- 17 B.-M. Jun, H. K. Lee and Y.-N. Kwon, *Chem. Eng. J.*, 2018, **332**, 419-430.
- 18 X. Guo, B. Zhao, L. Wang, Z. Zhang, J. Li and Z. Gao, *Sep. Purif. Technol.*, 2023, **325**, 124736.
- 19 Y.-L. Ji, Q.-F. An, X.-D. Weng, W.-S. Hung, K.-R. Lee and C.-J. Gao, *J. Membr. Sci.*, 2018, **548**, 559-571.
- 20 B. He, H. Peng, Y. Chen and Q. Zhao, *J. Membr. Sci.*, 2020, **608**, 118202.
- 21 B. Wu, N. Wang, J.-H. Lei, Y. Shen and Q.-F. An, *J. Membr. Sci.*, 2022, **643**, 120050.
- 22 X.-D. Weng, Y.-L. Ji, R. Ma, F.-Y. Zhao, Q.-F. An and C.-J. Gao, *J. Membr. Sci.*, 2016, **510**, 122-130.
- 23 B. Wu, N. Wang, Y. Shen, C.-G. Jin and Q.-F. An, *J. Membr. Sci.*, 2023, **666**, 121144.
- 24 T. Zhang, H. Zhang, P. Li, S. Ding and X. Wang, *Sep. Purif. Technol.*, 2022, **297**, 121541.